Symmetry breaking in a T-shaped photonic waveguide coupled with two identical nonlinear cavities

Evgeny Bulgakov[1,2] and Almas Sadreev[1]
[1]*Kirensky Institute of Physics, 660036, Krasnoyarsk, Russia*
[2]*Siberian State Aerospace University, Krasnoyarsk Rabochii, 31, Krasnoyarsk, Russia*
(Received 19 July 2011; published 12 October 2011)

We consider light transmission in a T-shaped photonic waveguide coupled with two identical symmetrically positioned nonlinear microcavities. We present two types of symmetry breaking. The first one is a result of mixing of the symmetric input wave with antisymmetric bound states in the Fabry-Pérot interferometer architecture. Similarly, the second mechanism of the symmetry breaking is the result of mixing the symmetrical input wave with the antibonding bound state in a straight waveguide coupled with two cavities positioned perpendicular to the waveguide. In both cases the mixing is due to nonlinearity. In turn, the symmetry-breaking solutions give rise to nonsymmetrical outputs in the T-shape waveguide. These effects are directly demonstrated by the electromagnetic field solutions which are complimented by coupled mode theory for the light transmission.

DOI: 10.1103/PhysRevB.84.155304 PACS number(s): 42.70.Qs, 41.20.Jb, 42.25.Bs, 42.65.Pc

I. INTRODUCTION

Symmetry breaking in a nonlinear quantum system is a fundamental effect caused by the interplay of nonlinearity with linear potential which defines the symmetry. It is commonly known that the ground state in one-dimensional linear quantum mechanics is nodeless and follows the symmetry of the potential. However, the self-attractive nonlinearity in the nonlinear Schrödinger equation breaks the symmetry of the ground state, replacing it by a new asymmetric state minimizing the systems energy. For example, the nonlinear Schrödinger equation in double-well potential reveals anti-symmetric ground state with variation of normalization of the state.[1] The phenomenon of the spontaneous symmetry breaking in analog with the double-well potential are realized in a nonlinear dual-core directional fiber.[2–4] Spontaneous symmetry breaking was demonstrated recently by Brazhnyi and Malomed in a linear discrete chain (Schrödinger lattice) with two nonlinear sites.[5] They have shown as analytically as well as numerically the existence of symmetric, antisymmetric, and nonsymmetric eigenmodes with eigenfrequencies below the propagation band of the chain, and that a variation of the population of modes can give rise to a bifurcation from one to another mode. The system can be applied to photonic crystal (PhC) waveguides with two in-channel nonlinear cavities.

A similar phenomenon of symmetry breaking occurs in the nonlinear system with injection of input power. That phenomenon is developed in nonlinear optics with the establishment of one or more asymmetric states which no longer preserve the symmetry properties of the original state.[6–10] In particular, Maes *et al*.[11,12] considered symmetry breaking for the nonlinear cavities aligned along the waveguide, that is a Fabry-Pérot architecture close to the system considered in Ref. 8. That system is symmetric relative to the inversion of the transport axis if equal power is injected on both sides of the coupled cavities. The symmetry breaking was found also for the case of many coupled nonlinear optical cavities in ringlike architecture.[13,14] The most simple underlying mechanism of the symmetry breaking in such a system was considered in Refs. 15 and 16 as an example of the optical guide coupled with two nonlinear off-channel cavities aligned symmetrically relative to the guide. For the linear case there are, at least, two eigenmodes of the coupled cavities, bonding (even symmetrical), and antibonding (odd antisymmetrical) ones. As we take the input light to be a symmetric wave relative to a mirror symmetry of the system, it is coupled with the bonding mode only. In other words, the antibonding mode cannot be excited by the input wave, and therefore it is the simplest bound state in continuum (BSC).[15,17,18] The mirror symmetry cannot be broken in the linear system. However, for the nonlinear cavities the principle of linear superposition is broken to give rise to a mixing of the antibonding mode with symmetrical light wave transmitted over the waveguide. Obviously, the mixing gives a total state which is neither symmetrical nor antisymmetrical, breaking the mirror symmetry. It was shown that the symmetry can be broken because of different light intensities or because of different phases of light oscillations at the cavities to provoke the Josephson-like current between cavities.[16]

In the present paper we consider the T-shaped photonic waveguide with two identical nonlinear cavities positioned symmetrically as shown in Fig. 1. That system combines two systems. The first one is the Fabry-Pérot interferometer (FPI) consising of two nonlinear off-channel cavities aligned along the straightforward waveguide considered in Refs. 11,12, and 19. As was shown in Ref. 19 there is a discrete set of the self-induced bound states in continuum (BSC) which are standing waves between off-channel cavities. We define these BSC as the FPI BSC below. In the second system two nonlinear cavities are aligned perpendicular to the input waveguide. As was said above there is the antibonding BSC. Here we show that both types of the BSC might be important for the breaking of symmetry. Preliminarily, we considered a simplified system in which the cavities were coupled only with output waveguides while the coupling with the input waveguide was disregarded.[20] With use of the coupled mode theory (CMT) all-optical switching based on the symmetry breaking was reported. For the case presented in Figs. 1(a) and 1(b) we show here that the mirror symmetry breaking is the result of mixing of the antisymmetric FPI BSC with the symmetric transport solution. However, with growth of the coupling of the cavities with the input waveguide the symmetry-breaking solution occurs because of the mixing of

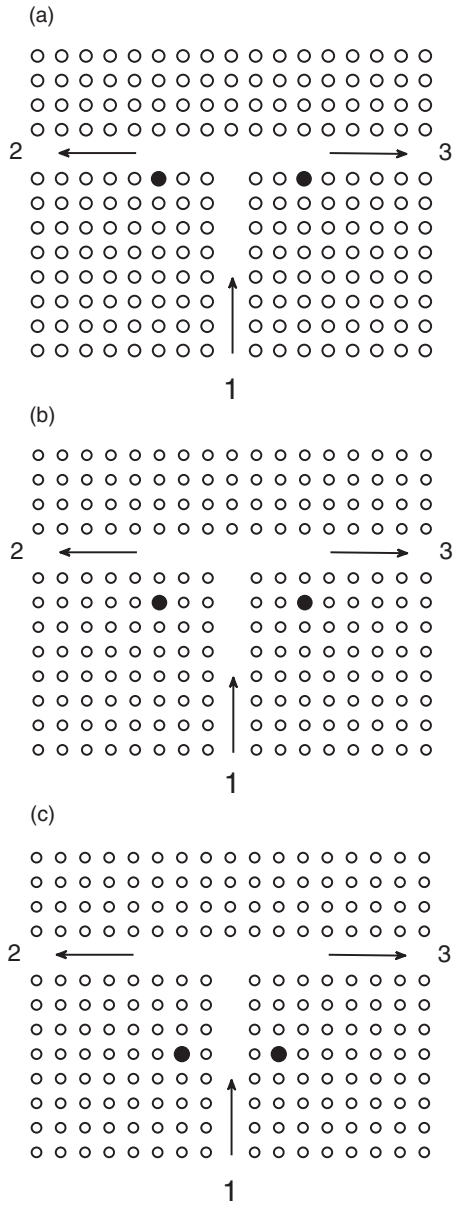

FIG. 1. Two defect rods made from a Kerr media marked by solid circles are inserted into the photonic crystal (PhC) of square lattice dielectric GaAs rods. The T-shape waveguide is formed by removing linear chains of GaAs rods. The cases (a)–(c) differ by the positions of the nonlinear defects.

the symmetrical transport solution with the antibonding BSC, too. That case corresponds to Fig. 1(c). The main aim is to demonstrate both mechanisms of the symmetry breaking by direct solution of the Maxwell equations complemented by the CMT consideration.

II. THE T-SHAPE PHOTONIC CRYSTAL WAVEGUIDE COUPLED WITH TWO NONLINEAR CAVITIES

We consider the PhC shown in Fig. 1 with the following parameters: the lattice constant $a = 0.5$ μm, the cylindrical dielectric rods have radius $0.18a$, and dielectric constant $\epsilon_0 = 11.56$ (GaAs at the wavelength 1.5 μm in air). Removing a row of rods fabricates the PhC waveguide.[19,21] The waveguide supports a single band of guided TM mode spanning from the bottom band edge 0.315 to the upper one 0.41 in terms of $2\pi c/a$. We substitute two defect rods of the same radius as shown in Fig. 1 made from an instantaneous Kerr media with the nonlinear refractive index $n = n_0 + n_2 I$ where $n_0 = \sqrt{3}$ and $n_2 = 2 \times 10^{-12}$ cm$^2/W$; I is the light intensity averaged over the cross section of the thin defect rods.

We start with the position of the defect rods shown in Fig. 1(a) which have strong coupling with the output waveguides 2 and 3, and negligibly weak coupling with the input waveguides 1. The Maxwell equations for the TM mode in the PhC have the following form:

$$\left\{\nabla^2 + \frac{\omega^2}{c^2}[\epsilon(\mathbf{r}) + \delta\epsilon(\mathbf{r})]\right\} E(\mathbf{r}) = 0, \quad \epsilon(\mathbf{r} + \mathbf{R}) = \epsilon(\mathbf{r}), \tag{1}$$

where $\mathbf{R} = a(j\mathbf{e}_x + m\mathbf{e}_y)$ runs over cells of a square lattice of rods. $\mathbf{e}_x$,$\mathbf{e}_y$ are the unit vectors of the square lattice. The dielectric constant is considered to be $\epsilon(\mathbf{r}) = \epsilon_0$ inside the rods and unit outside. Two terms contribute into the second expression $\delta\epsilon(\mathbf{r})$. The first one is due to removing straight rows of dielectric rods to form the T-shaped waveguide. Two defect rods made from a Kerr media give the second contribution in the form $(n_0 + n_2 I)^2 - \epsilon_0$ provided that the radius $\mathbf{r}$ belongs to the defect rods. By an expansion of electromagnetic field over maximally localized photonic Wannier functions[21,22] the effective model on a squared lattice can be formulated. Taking the solution as incident wave injected into the input waveguide 1, reflected and transmitted far from the scattering region the solution inside the scattering region can be written in the Lippman-Schwinger equation form:[23]

$$(\omega - H_{\text{eff}})|\Psi_S\rangle = E_{\text{in}}\hat{V}|inc\rangle. \tag{2}$$

Here H_{eff} is the effective non-Hermitian Hamiltonian which is the result of the Feshbach procedure of the projection of the total hHermitian Hamiltonian onto a subspace of discrete eigenstates of the closed scattering region.[24–29] $|\Psi_S\rangle$ is the scattering wave function inside the scattering region, $|inc\rangle$ is the wave function that describes the incident wave with the electric field amplitude E_{in}, and $\hat{V}$ is the coupling matrix of the PhC waveguide with the scattering region. Details of derivation of this equation are given in Ref. 23. Equation (2) is similar to CMT equations,[30–34] however, in the case of real PhC the scattering state $|\Psi_S\rangle$ includes around a hundred cells inside the scattering region just as shown in Fig. 1. This is the only way if we need to find the scattering wave function.

The case of the T-shaped structure shown in Figs. 1(a) and 1(b) has an analogy with the Fabry-Pérot interferometer (FPI) comprising two off-channel nonlinear cavities. As was shown in Ref. 19 there are a series of the bound states in continuum (BSC) which are standing waves between the off-channel cavities. It was shown that the BSC exists for any distance between the off-channel defect rods because of their nonlinearity.[19] Similar BSC solutions are expected to exist in the present case of the T-shaped waveguide coupled with two off-channel cavities shown in Fig. 1(a). However, these solutions are to be standing waves with nodes at the point of connection of all waveguides. Therefore in the present

FIG. 2. (Color online) (Color online) The solution of Maxwell equations for the case shown in Fig. 1(a) which demonstrates the antisymmetric FPI BSC (antisymmetric standing wave between nonlinear off-channel defects marked by stars) with frequency $\omega_c a/2\pi c = 0.3402$. Only that part of the PhC is shown where the scattering wave function Ψ_S is given in the Lippmann-Schwinger Eq. (2).

case the BSCs are the antisymmetric states only. Figure 2 shows one of these antisymmetric standing waves in the T-shaped waveguide with two nonlinear defect rods with the eigenfrequency $\omega_c a/2\pi c = 0.3402$ which satisfies the condition $3k(\omega_c)a = \pi$.

For the linear case, the BSC has zero coupling with the symmetric EM wave which inputs in the waveguide 1. Therefore the general solution of the Lippmann-Schwinger Eq. (2) is the linear superposition of the transport solution given by the right term in the equation and the BSC with the arbitrary superposition coefficient.[23,35] For the nonlinear cavities there is no principle of the linear superposition. Nonlinearity gives rise to an important effect of the excitation of BSC by transmitted wave (i.e., an interaction between the antisymmetric BSC and the symmetric transmitted wave). As a result the total solution lacks the mirror symmetry of the PhC structure shown in Fig. 1(a). That is one of the scenarios of the symmetry breaking. Note that Maes *et al.*[11] have already reported the symmetry breaking in the FPI. In order for the FPI with two off-channel nonlinear cavities to have the mirror symmetry, equal input power must be applied to both sides of the FPI.[11] In our case of the T-shaped waveguide this symmetry is achieved by application of the input power via the additional waveguide positioned at the center of the FPI.

Figure 3(a) demonstrates the solution for the light intensities of the cavities $I_j = c|E_j|^2/8\pi, j = 1,2$ with broken mirror symmetry where E_j are the amplitudes of the electric field in thin defect rods for two values of input power. The solution converges to the BSC point marked by the star if the input power limits to zero. At this point the symmetry is restored. As a result for the input power $P \neq 0$ the light transmission from the input waveguide 1 to the left waveguide 2 differs from the transmission and to the right waveguide 3 as seen from Fig. 3(b). Moreover, the difference $T_L - T_R$ crucially depends on the frequency in the vicinity of the BSC point. Figure 4 demonstrates the solution of the Maxwell equations for the z component of electric field (scattering wave function)

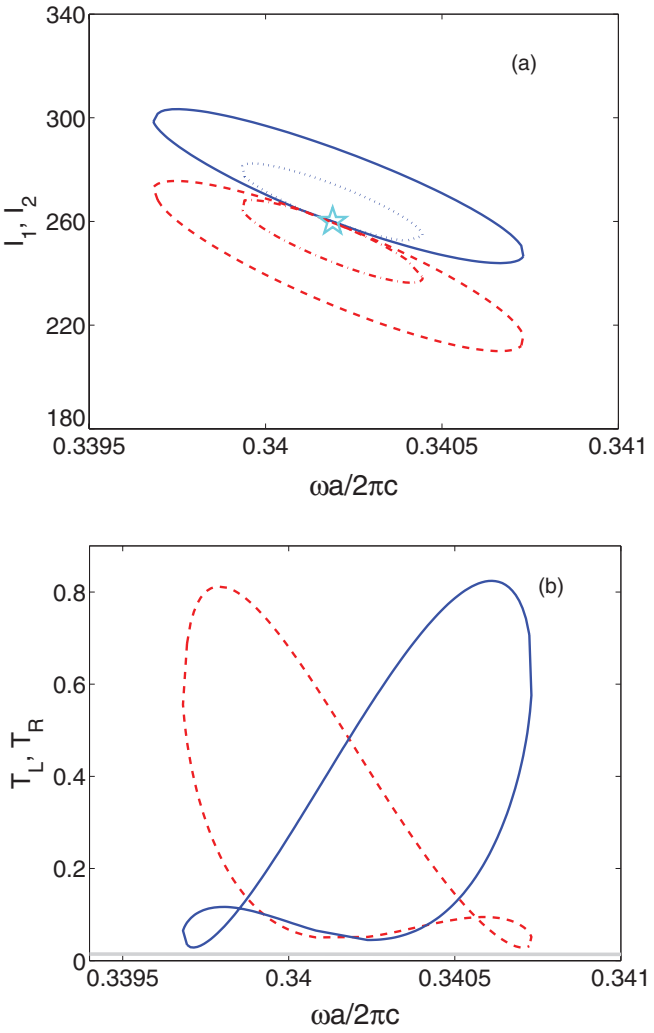

FIG. 3. (Color online) (a) The frequency behavior of light intensities at the defect rods given in terms of W/a^2. Dotted blue and dash-dotted red lines correspond to the input power equal to $0.48W/a$; solid blue and dashed red lines correspond to $1.92W/a$. Only that solution for intensities is shown which breaks the symmetry. (b) The frequency dependence of the transmissions to the left T_L (blue solid lines) and to the right T_R (red dashed lines) for the PhC T-shaped waveguide shown in Fig. 1(a). The BSC point is shown by the blue star.

breaks the mirror symmetry because of mixing the symmetric input wave with the antisymmetric BSC shown in Fig. 2. The intensity of the defect's modes is centered around the BSC intensity which is rather large as shown in Fig. 3(a) while the incident light intensity $P \sim 1 \cdot W/a$. Thereby we have chosen exponential scaling for the solution of the Maxwell equations presented in Fig. 4 in order to distinguish waves in waveguides.

As was shown in the framework of the CMT there might appear an additional branch of a loop shape for the symmetry-breaking solution with growth of the input power.[20] The numerical results for a solution of the Maxwell equations completely agree with these model results as seen from Fig. 5(a) by dotted brown and green lines. The loops shown by dotted lines in Fig. 5 are the result of individual instability that

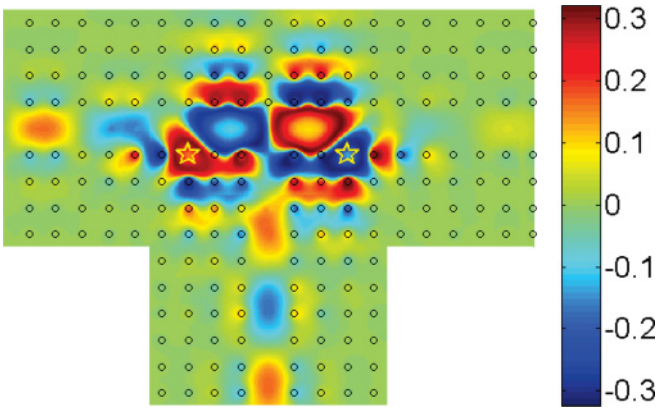

FIG. 4. (Color online) The symmetry-breaking EM field solution in a scale $real(E_z)\exp(-|E_z|)$ for $P = 1.94W/a$ and $\omega a/2\pi c = 0.3402$ (the BSC frequency). Light is incident into the 1 waveguide and scatters to the left and right waveguides 2 and 3 with $T_L = 0.8236, T_R = 0.0560$.

arises for transmission in the left or right waveguide coupled with the left or right nonlinear off-channelcavity.[20] Loops in the intensities are reflected in the loops in the transmission for the transmission to the left and for the transmission to the right as shown in Fig. 5(b) by dotted brown and green lines, respectively. With further growth of the input power the domain of existence of this symmetry-breaking branch is increased providing almost complete blocking of the output into the right waveguide as shown in Fig. 6.

Bistability of the light transmission in the PhC waveguide coupled with the nonlinear optical cavity crucially depends on the coupling: the smaller a coupling the less input power is needed for bistability.[36] For case (a) in Fig. 1 the coupling is rather large to observe bistability in the transmission. However, case (b) has the sufficiently smaller coupling as one can see from Table I. As a result the case in Fig. 1(b) gives rise to additional loops as shown in Fig. 5 for larger input power $5.57W/a$. Figure 7 shows the wave function for the symmetry-preserving solution (a) and the symmetry-breaking solution (b) and (c). The cases (b) and (c) differ by the frequency. One can see from Figs. 7(a) and 7(b) that for the symmetric solution the transmission excites the cavities weakly, while for the symmetry-breaking solution the cavities are strongly excited because of mixing with the antisymmetric FPI BSC. Figure 7(c) shows that for the frequency in the loop domain $\omega a/2\pi c = 0.3442$ the first nonlinear cavity is excited much more than the second one that is correlated with the outputs.

The T-shaped waveguide coupled with two nonlinear cavities shown in Fig. 1 is remarkable in that it allows the limit to the FPI [cases (a) and (b)] with the FPI BSC in the form of standing waves between two off-channel defects[19] as well as the limit to case (c) in Fig. 1 with the BSC in the form of the antibonding defect's state. Patterns of such antibonding BSC in PhC straight waveguide coupled with two cavities positioned perpendicular to the waveguide is shown in Fig. 8. Patterns of that BSC also are shown in Refs. 15 and 23. The nonlinearity gives rise to mixing the antibonding BSC with the wave transmitted over waveguide 1. For the linear defect rods this state would be the perfect BSC. For the nonlinear

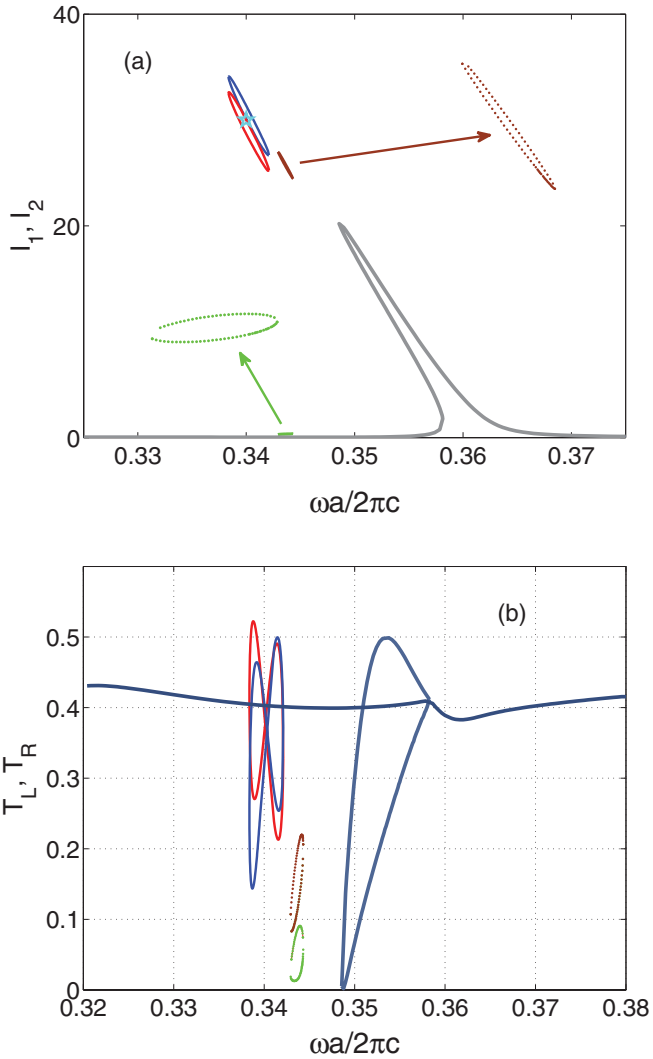

FIG. 5. (Color online) The frequency behavior of (a) the light intensities at the defect rods (in terms of $I_0 = W/a^2$) and (b) transmissions T_L and T_R for the PhC T-shaped waveguide shown in Fig. 1(b). The input power equals $5.57W/a$. The symmetric solution is shown by the solid gray line which inherits the linear case. The symmetry-breaking solution because of the mixing of the symmetric transport solution with the antisymmetric BSC is shown by solid blue and red lines. The next symmetry-breaking solution because of a bistability of the transmission in each output waveguide is shown by dotted brown and green lines.

cavities mixing this antibonding BSC with symmetric input light leads to the breaking of the mirror symmetry to give rise to the breaking of symmetry in the input waveguide. Then for the evolution of this structure to the T-shaped case, one can expect different outputs to the right and to the left. Indeed, in spite of the small difference of the defect intensities presented in Fig. 9(a) the transmissions T_L and T_R demonstrate a vast difference including the case of almost perfect blocking of the transmission to the left as shown in Fig. 9(b) for $\omega a/2\pi c = 0.3505$. Figure 10 shows the antibonding BSC is mixed to the transport over the input waveguide to give rise to the symmetry-breaking solution.

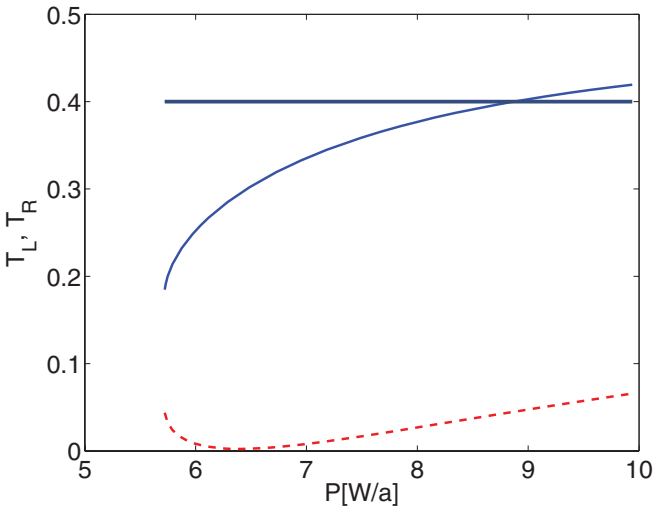

FIG. 6. (Color online) Output intensities to the left and right waveguides as dependent on the input power for the case Fig. 1(b) and $\omega a/2\pi c = 0.344$. The gray line shows the symmetry-breaking solution, solid and dashed lines show the symmetry-breaking solution.

III. COUPLED MODE EQUATIONS

As was said above the Maxwell theory of the light propagation in the PhC waveguide coupled with two defect rods includes more than a hundred sites shown by open circles in Figs. 2, 4, and 7. Even for a stationary process of the light transmission the self-consistent solution of a hundred algebraic nonlinear equations for the case of two nonlinear defect rods is a rather time-consuming task. Moreover the nonstationary transmission as well as the problem of establishment of stable solutions become a formidable problem. Therefore in this section we explore the CMT equations which include only the degrees of freedom of two nonlinear defect modes. To the best our knowledge the first formulation of the CMT was done by Snyder[37,38] for consideration of the EM wave propagation in nonuniform media and in optical fibers by separation of the total system onto the modes associated with both the discrete and continuous eigenvalue spectrum with further expulsion of continuous modes. We note that the idea was first formulated and realized by Livsic[24] and independently by Feshbach[25] by use of the projection operator technique to formulate the idea of the non-Hermitian effective Hamiltonian. For the present system we use the CMT formulated in Refs. 33 and 34. Thus, following Ref. 34 we consider a light given by the amplitude S_{1+} is incident into waveguide 1 and outputs into all three terminals as shown schematically in Fig. 11. The outgoing amplitudes are labeled as S_{1-}, S_{2-}, and S_{3-}. Each nonlinear optical cavity is assumed to be given by single-mode

TABLE I. Parameter sets of the CMT for PhC T-shaped waveguide shown in Fig. 1.

Type of structure in Fig. 1	(a)	(b)	(c)
Γ (in terms of $a/2\pi c$)	0.0002	0.0002	0.00189
γ (in terms of $a/2\pi c$)	0.03093	0.00189	0.00002
ω_0 (in terms of $a/2\pi c$)	0.3609	0.365	0.3596

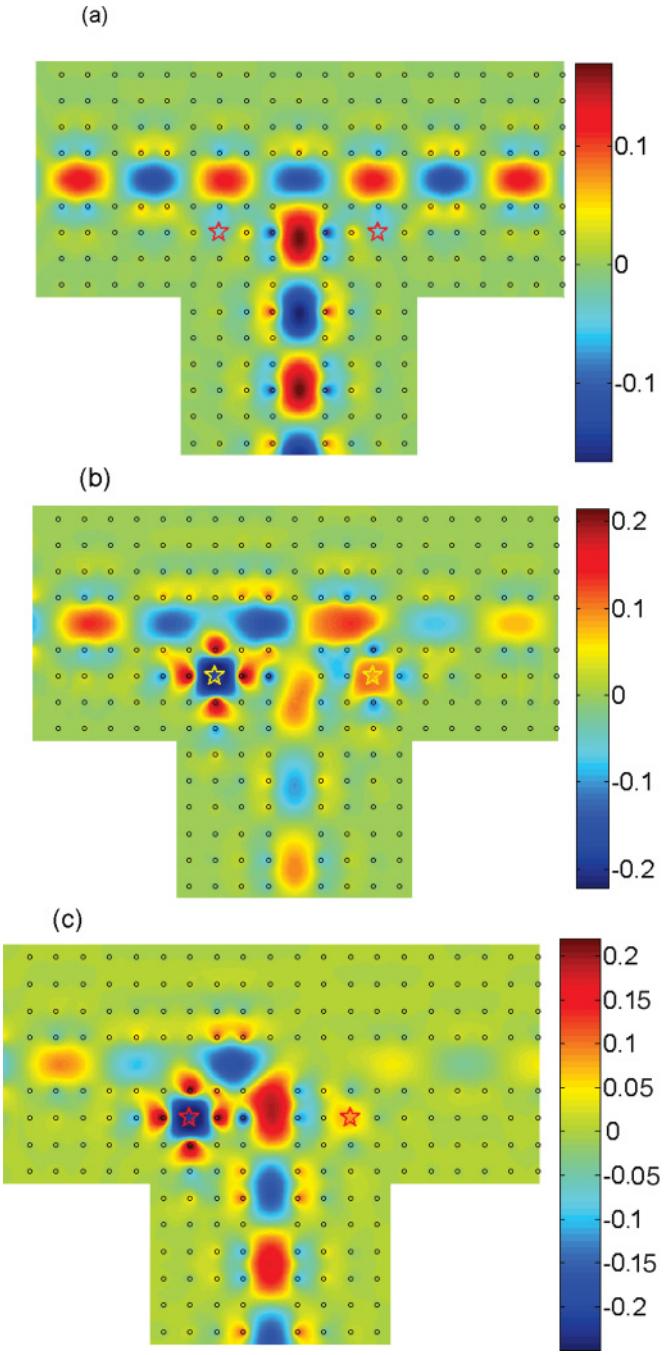

FIG. 7. (Color online) The EM field solution in a scale $real(E_z)\exp(-|E_z|)$ for (a) the symmetry-preserving solution for $\omega a/2\pi c = 0.3442$, (b) the symmetry-breaking solution caused by the BSC for $\omega a/2\pi c = 0.3388$, and (c) for $\omega a/2\pi c = 0.3442$.

amplitudes $A_j, j = 1,2$ and coupled with guides 2 and 3 via the coupling constant γ shown in Fig. 11 by dotted lines and with guide 1 via the coupling constant Γ.

$$\begin{aligned}(\omega - \omega_1 + i\gamma + i\Gamma)A_1 + i\Gamma A_2 &= i\sqrt{\Gamma}(S_{1+} + \sigma_{1-}e^{i\theta}) + i\sqrt{\gamma}\sigma_{2-}e^{i\phi},\\ (\omega - \omega_2 + i\gamma + i\Gamma)A_2 + i\Gamma A_1 &= i\sqrt{\Gamma}(S_{1+} + i\sigma_{1-}e^{i\theta}) + i\sqrt{\gamma}\sigma_{3-}e^{i\phi},\end{aligned} \quad (3)$$

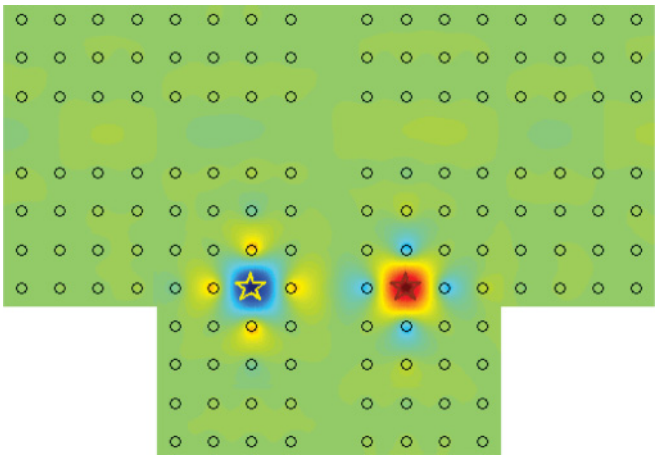

FIG. 8. (Color online) The solution of Maxwell equations for the case shown in Fig. 1(c) which demonstrates the antibonding BSC (antisymmetric mode) localized mostly at the defects marked by stars with frequency $\omega_c a/2\pi c = 0.3478, n_0 = 1.94$.

where the eigenfrequencies of the nonlinear optical cavities (defects) are shifted because of the Kerr effect.

$$\omega_j = \omega_0 + \lambda |A_j|^2, \quad j = 1,2. \tag{4}$$

Here phases θ and ϕ as shown in Fig. 11 are the optical lengths through which light goes between the connections.

These CMT equations are to be complemented by the equations for light amplitudes at each connection A, B, and D,

$$\begin{aligned} \sigma_{1+}e^{-i\theta} &= S_{1+} - \sqrt{\Gamma}(A_1 + A_2), \\ S_{1-} &= \sigma_{1-}e^{i\theta} - \sqrt{\Gamma}(A_1 + A_2), \\ S_{2-} &= \sigma_{2-}e^{i\phi} - \sqrt{\gamma}A_1, \\ S_{3-} &= \sigma_{3-}e^{i\phi} - \sqrt{\gamma}A_2, \\ \sigma_{2+}e^{-i\phi} &= -\sqrt{\gamma}A_1, \\ \sigma_{3+}e^{-i\phi} &= -\sqrt{\gamma}A_2. \end{aligned} \tag{5}$$

The T connection at the C point connects ingoing and outgoing amplitudes by the S matrix as follows:

$$\begin{pmatrix} \sigma_{1-} \\ \sigma_{2-} \\ \sigma_{3-} \end{pmatrix} = \begin{pmatrix} a & b & b \\ b & c & d \\ b & d & c \end{pmatrix} \begin{pmatrix} \sigma_{1+} \\ \sigma_{2+} \\ \sigma_{3+} \end{pmatrix}. \tag{6}$$

In particular, the solution of the Maxwell equations for the T-shaped waveguide without defects gives the matrix elements of the S matrix (6) $a = -0.3547 + 0.308i, b = 0.6 + 0.173i, c = -0.4319 + 0.2271i, d = -0.568 + 0.2225i$ at $\omega a/2\pi c = 0.35$. Equations (3), (5), and (6) form a full system of equations for 11 amplitudes $A_1, A_2, \sigma_{1+}, \sigma_{1-}, \sigma_{2+}, \sigma_{2-}, \sigma_{3+}, \sigma_{3-}, S_{1-}, S_{2-}, S_{3-}$. Substituting $S_{1+} = E_{\text{in}}e^{i\omega t}, A_{1,2} = A_{1,2}e^{-i\omega t}$ we obtain after some algebra the following stationary CMT equations:

$$(\omega - H_{\text{eff}}) \begin{pmatrix} A_1 \\ A_2 \end{pmatrix} = i E_{\text{in}} F \begin{pmatrix} 1 \\ 1 \end{pmatrix}, \tag{7}$$

where

$$H_{\text{eff}} = \begin{pmatrix} \omega_1 - iG & -iH \\ -iH & \omega_2 - iG \end{pmatrix}, \tag{8}$$

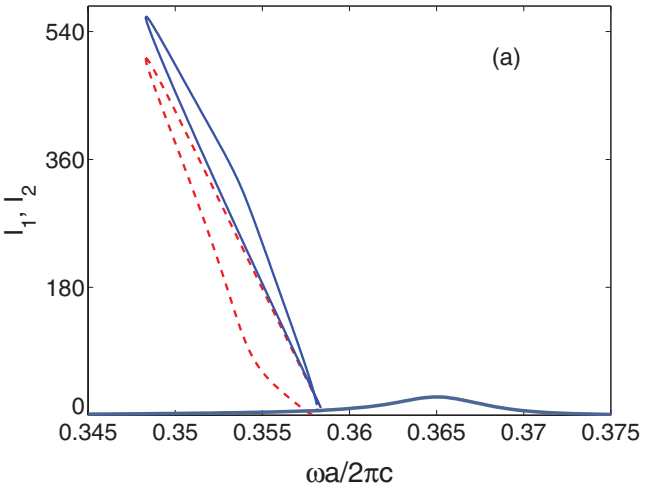

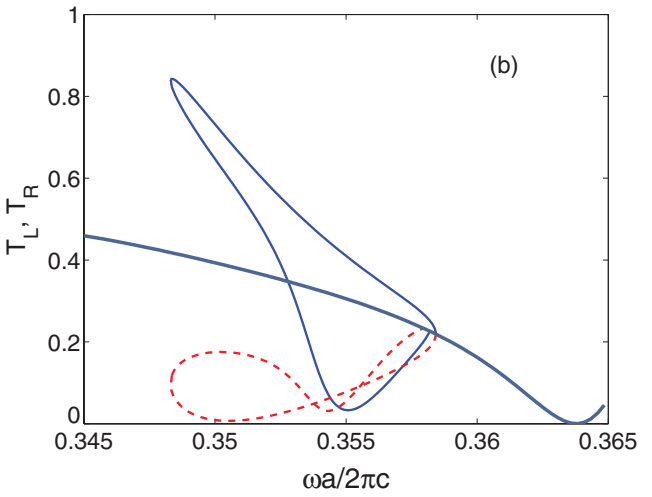

FIG. 9. (Color online) The frequency behavior of (a) the light intensities at the defect rods and (b) transmissions T_L and T_R for the PhC T-shaped waveguide shown in Fig. 1(c). The input power $P = 0.48W/a$. Only the solution is shown in (b) which demonstrates different outputs in the left (red dashed line) and right (blue solid line) waveguides.

$$\begin{aligned} G &= \gamma + \Gamma(1 + ae^{2i\theta}) + \gamma de^{2i\phi} + \sqrt{\gamma\Gamma}(b + c)e^{i\theta + i\phi}, \\ H &= \Gamma + \sqrt{\gamma\Gamma}(b + c)e^{i\theta + i\phi} + \Gamma ae^{2i\theta} + \gamma de^{2i\phi}, \\ F &= \sqrt{\Gamma}(1 + ae^{2i\theta}) + \sqrt{\gamma}be^{i(\theta+\phi)}. \end{aligned} \tag{9}$$

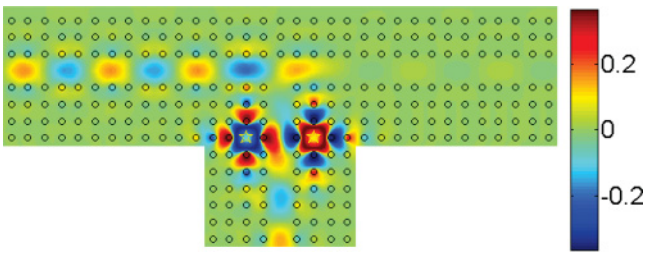

FIG. 10. (Color online) The EM field for the symmetry-breaking solution $\omega a/2\pi c = 0.3505$. Light is incident into the 1 waveguide and scatters to the left and right waveguides 2 and 3. $P = 0.48W/a$.

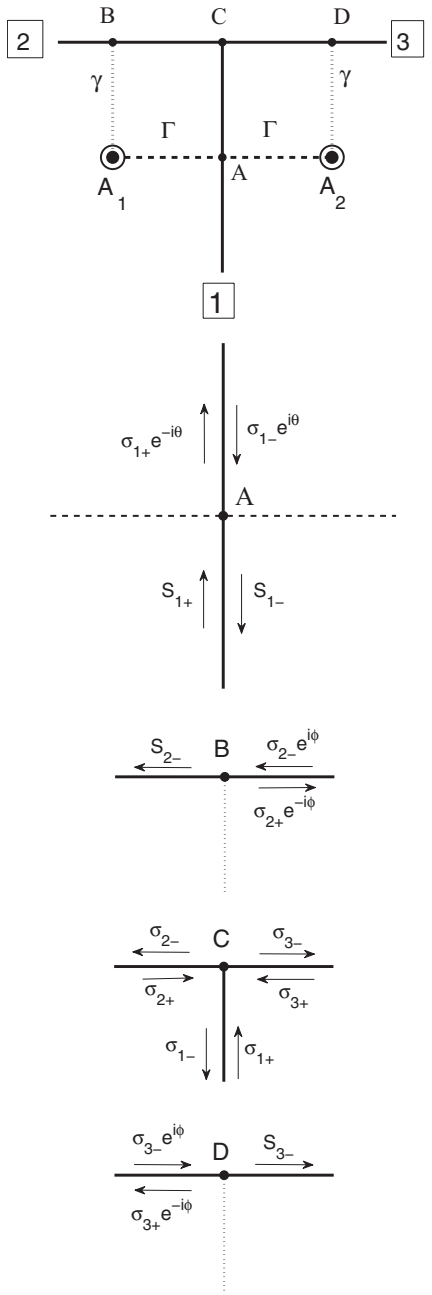

FIG. 11. (a) CMT model of the T-shape photonic crystal waveguide coupled with two nonlinear optical cavities made from Kerr media shown by solid bold circles. The last are coupled with input waveguide 1 via the constant Γ shown by dashed lines and with the output waveguides 2,3 via the constant γ shown by the dotted line. Separately each connection is shown with corresponding light amplitudes.

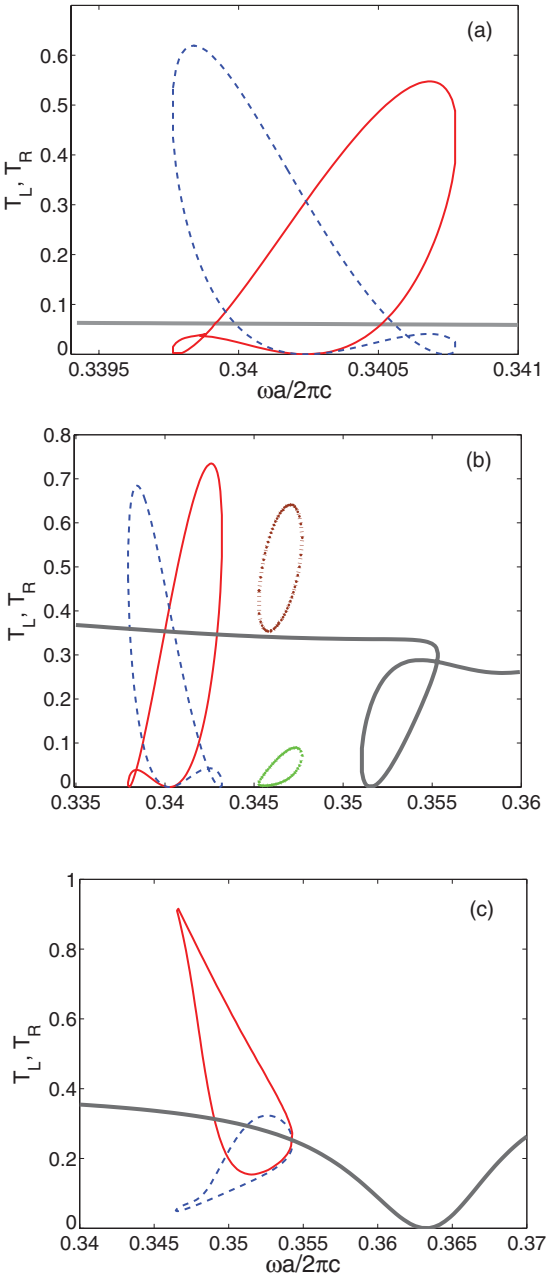

FIG. 12. (Color online) The frequency behavior of the transmissions T_L (blue dashed line) and T_R (solid red line) from the input waveguide 1 into the output ones 2 and 3, respectively. The gray thick line shows the symmetry-preserving solution. (a) $P = 1.92W/a, \Gamma = 0.0002, \gamma = 0.031$ that exactly corresponds to the case shown in Fig. 1(a). (b) $P = 5.57W/a, \Gamma = 0.0002, \gamma = 0.00189$ that exactly corresponds to the case shown in Fig. 1(b). New branch in loop shape is shown by dotted lines, brown for T_R and green for T_L. (c) $P = 0.48W/a, \Gamma = 0.00189, \gamma = 0.00002$ that exactly corresponds to the case shown in Fig. 1(c).

One can see that the CMT equations (7) are similar to the Lippmann-Schwinger equation (2), however, with a significant difference. For the CMT equations the rank of the matrix H_{eff} equals the number of nonlinear defects.

We can explicitly calculate all necessary parameters for the present PhC in order to substitute them into the CMT. By calculation of the light transmission in the straight waveguide coupled with the single linear off-channel defect positioned at different positions we are able to extract the coupling constant of the cavity with the PhC waveguide Γ and the eigenfrequency of monopole mode ω_0. The results are collected in Table I. The limiting case of the T-shaped waveguide with $\Gamma = 0$ is considered in Ref. 20 with results qualitatively close to those shown in Figs. 3 and 5. Here we find the solutions of nonlinear CMT equations (7) with the substitution of concrete

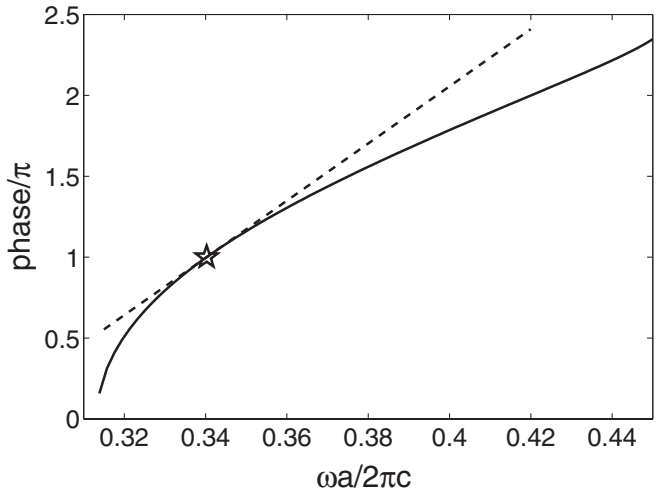

FIG. 13. The frequency behavior of the optical length (phase) shown by solid line for the straight PhC waveguide which is fabricated by removing of one row of dielectric rods. The parameters of the PhC are listed in the caption for Fig. 1. The BSC point is marked by the star.

parameters listed in Table I and present the output light transmission to the left and to the right waveguides. We start with the case shown in Figs. 1(a) and 12(a).

Moreover, we present the real dispersion curve $\omega(k)$ calculated for the straight PhC waveguide and find the optical length given by phase θ or ϕ depends on frequency ω. This curve is shown in Fig. 13 by the solid curve for the parameters of PhC given in Fig. 1. In the vicinity of the BSC frequency $\omega_c a/2\pi c = 0.3402$ we approximate the dispersion curve as linear to obtain

$$\frac{\text{phase}}{\pi} = 1 + \frac{17.68(\omega - \omega_c)a}{2\pi c}, \tag{10}$$

parameters for the phases.

IV. SUMMARY AND CONCLUSIONS

By direct solution of the Maxwell equation (2) we considered electromagnetic transmission in the T-shaped photonic crystal waveguide for three different symmetric positions of two identical off-channel nonlinear cavities as shown in Fig. 1. For the case of cavities weakly coupled with the input waveguide [Figs. 1(a) and 1(b)] we demonstrate the solution in the form of a standing wave trapped between the cavities which is the FPI BSC with a fixed value of intensity and frequency of oscillations for the limit of small input power. This BSC differs from the BSC in the FPI only in that it is to be the antisymmetric one relative to the mirror symmetry of the T-shaped waveguide as shown in Fig. 2 in order to exclude leakage into the input waveguide 1. However as soon as the input power is not equal to zero the antisymmetric BSC couples with the symmetric transport solution because of a lack of the superposition principle in the nonlinear quantum system. That process of the symmetry breaking is demonstrated in Fig. 7(b). Thus, the antisymmetric BSC ceased to be in hidden mode allowing for the symmetric input wave to give rise to the resonance of a rather unusual butterfly shape as was shown in Fig. 3(b) with strong asymmetry of outputs to the left and to the right. This consideration was complimented by the CMT equations with parameters found directly for the two-dimensional PhC structure and collected in Table I. The CMT solution shown in Fig. 12(a) agrees with the numerical solution of the Maxwell equations presented in Fig. 3(b).

For strong asymmetry of outputs we found that the symmetry-breaking solution is developed in the form of separated loops as shown in Fig. 5(a) by dotted lines if the input power exceeds the threshold. It results in additional loops in the transmission onto right and left output waveguides as shown in Fig. 5(b). Correspondingly, the strong asymmetry is seen in the EM field solution shown in Fig. 7(c). As shown in Fig. 9 the left or right light output might be almost completely blocked with variation of the input power. That result is the most important for all-optical switching of outputs in the T-shape waveguide.[20]

If the couplings of the nonlinear off-channel cavities with the input waveguide (denoted by Γ in Fig. 11) exceed the couplings of the cavities with the output waveguides (denoted by γ in Fig. 11) the antibonding BSC might appear as shown in Fig. 8. Once more, as soon as the input power is applied through guide 1 this BSC mixes with the symmetric input wave to destroy the BSC because of nonlinearity.[15,16] That phenomenon defines the second mechanism of the symmetry breaking as demonstrated in Figs. 9 and 10. The CMT consideration shown in Fig. 12(c) also confirms this mechanism of the symmetry breaking, however, one can notice that the agreement is only qualitative. We consider that disagreement is related in that the nonlinear off-channel cavities in Fig. 1(c) have direct coupling between each other. As shown in Ref. 15 that gives rise to significant different results compared to the case without coupling of the cavities.

ACKNOWLEDGMENTS

A.S is grateful to Boris Malomed for fruitful discussions about symmetry breaking. The work is partially supported by RFBR grant 12-02-00483.

[1]E. A. Ostrovskaya, Y. S. Kivshar, M. Lisak, B. Hall, F. Cattani, and D. Anderson, Phys. Rev. A **61**, 031601 (2000); R. D Agosta, B. A. Malomed, and C. Presilla, Phys. Lett. A **275**, 424 (2000).

[2]N. Akhmediev and A. Ankiewicz, Phys. Rev. Lett. **70**, 2395 (1993).

[3]R. Tasgal and B. A. Malomed, Phys. Scr. **60**, 418 (1999).

[4]A. Gubeskys and B. A. Malomed, Eur. Phys. J. D **28**, 283 (2004).

[5]V. A. Brazhnyi and B. A. Malomed, Phys. Rev. A **83**, 053844 (2011).

[6]M. Haelterman and P. Mandel, Opt. Lett. **15**, 1412 (1990).

[7]T. Peschel, U. Peschel, and F. Lederer, Phys. Rev. A **50**, 5153 (1994).

[8]I. V. Babushkin, Yu. A. Logvin, and N. A. Loiko, Quant. Electron. **28**, 104 (1998).
[9]J. P. Torres, J. Boyce, and R. Y. Chiao, Phys. Rev. Lett. **83**, 4293 (1999).
[10]L. Longchambon, N. Treps, T. Coudreau, J. Laurat, and C. Fabre, Opt. Lett. **30**, 284 (2005).
[11]B. Maes, M. Soljaĉić, J. D. Joannopoulos, P. Bienstman, R. Baets, S-P. Gorza, and M. Haelterman, Opt. Express **14**, 10678 (2006).
[12]B. Maes, P. Bienstman, and R. Baets, Opt. Express **16**, 3069 (2008).
[13]K. Otsuka and K. Ikeda, Opt. Lett. **12**, 599 (1987).
[14]K. Huybrechts, G. Morthier, and B. Maes, J. Opt. Soc. Am. B **27**, 708 (2010).
[15]E. N. Bulgakov, K. N. Pichugin, and A. F. Sadreev, Phys. Rev. B **83**, 045109 (2011).
[16]E. N. Bulgakov, K. N. Pichugin, and A. F. Sadreev, J. Phys. Condens. Matter **23**, 065304 (2011).
[17]M. L. Ladron de Guevara, F. Claro, and P. A. Orellana, Phys. Rev. B **67**, 195335 (2003).
[18]E. N. Bulgakov and A. F. Sadreev, Phys. Rev. B **80**, 115308 (2009).
[19]E. N. Bulgakov and A. F. Sadreev, Phys. Rev. B **81**, 115128 (2010).
[20]E. N. Bulgakov and A. F. Sadreev, J. Phys. Cond. Mat. **23**, 315303 (2011).
[21]K. Busch, S. F. Mingaleev, A. Garcia-Martin, M. Schillinger, and D. Hermann, J. Phys. Condens. Matter **15**, R1233 (2003).
[22]N. Marzari and D. Vanderbilt, Phys. Rev. B **56**, 12847 (1997).
[23]E. N. Bulgakov and A. F. Sadreev, Phys. Rev. B **78**, 075105 (2008).
[24]M. S. Livsic, Sov. Phys. JETP **4**, 91 (1957).
[25]H. Feshbach, Ann. Phys. (NY) **5**, 357 (1958); **19**, 287 (1962).
[26]I. Rotter, Rep. Prog. Phys. **54**, 635 (1991).
[27]V. V. Sokolov and V. G. Zelevinsky, Ann. Phys. **216**, 323 (1992).
[28]S. Datta, *Electronic Transport in Mesoscopic Systems* (Cambridge University Press, Cambridge, 1995).
[29]A. F. Sadreev and I. Rotter, J. Phys. A: Math. Gen. **36**, 11413 (2003).
[30]H. A. Haus, *Waves and Fields in Optoelectronics* (Prentice-Hall, New York, 1984).
[31]P. R. Villeneuve, S. Fan, and J. D. Joannopoulos, Phys. Rev. B **54**, 7837 (1996).
[32]C. Manolatou, M. J. Khan, S. Fan, P. R. Villeneuve, H. A. Haus, and J. D. Joannopoulos, IEEE J. Quantum Electron. **35**, 1322 (1999).
[33]S. Fan, W. Suh, and J. D. Joannopoulos, J. Opt. Soc. Am. A **20**, 569 (2003).
[34]W. Suh, Z. Wang, and S. Fan, IEEE J. Quantum Electron. **40**, 1511 (2004).
[35]E. N. Bulgakov, K. N. Pichugin, A. F. Sadreev, and I. Rotter, JETP Lett. **84**, 508 (2006).
[36]J. Joannopoulos, S. G. Johnson, J. N. Winn, and R. D. Meade, *Photonic Crystals: Molding the Flow of Light* (Princeton University Press, Princeton, 2008).
[37]A. W. Snyder, IEEE Microwave Theor. Tech. **18**, 383 (1970).
[38]A. W. Snyder, J. Opt. Soc. Am. **62**, 1267 (1972).